Sensors & Actuators: B. Chemical 276 (2018) 271–278

Contents lists available at ScienceDirect

Sensors and Actuators B: Chemical

journal homepage: www.elsevier.com/locate/snb

Photonic crystal surface mode imaging biosensor based on wavelength interrogation of resonance peak

Valery N. Konopsky*, Elena V. Alieva

Institute of Spectroscopy, Fizicheskaya, 5, Troitsk, Moscow 108840, Russia

ARTICLE INFO

Keywords:
Label-free optical biosensors
Surface wave imaging
Photonic crystal surface modes

ABSTRACT

A novel biosensing technique with a two-dimensional (2D) visualization, which is based on photonic crystal surface modes (PC SMs), is presented. The 2D image of the surface with picometer thickness resolution can be obtained when the PC chip under study is placed between crossed polarizers to convert a PC SM resonance dip into a resonance peak. The PC chip is designed so that the PC SM resonance peak is located between the maxima of the blue and green pixels of a color camera. The spectral shift of the resonance peak is determined by balancing of the intensities of the blue and green pixels at each point in the color camera. The spatial distribution of resonance wavelength shifts across the camera reflects the spatial distribution of changes in the thickness of the adsorbate over the sample. The spatial resolution of the resulting 2D image is determined by the propagation length of the PC surface wave.

1. Introduction

Label-free optical biosensors play an important role in the selective recognition of target biomolecules and in biomolecular interaction analysis, providing kinetic data about biological binding events in real time without labeling. The most popular label-free methods use the propagation of some optical surface wave along a bioactive surface to detect the binding of the analyte with ligands on the surface [1]. For example, in the surface plasmon resonance (SPR) technique, this surface-bound wave is a surface plasmon-polariton that propagates along a gold or silver surface [2]. At present, most commercial label-free optical biosensors are based on the SPR method.

In a more recent alternative to the SPR method, the surface-bound wave is an excitation of a photonic crystal surface mode (PC SM). In this method, confinement of the optical field near the interface results from the photonic band gap in the multilayer structure on the internal side of the outer surface and from total internal reflection on the external side, which is in contact with the liquid. These PC SMs, which are also called 'photonic band-gap surface modes', 'modes of (asymmetric) planar Bragg waveguide', 'surface waves in periodic layered medium', 'photonic crystal surface waves', 'optical Bloch surface waves', and 'surface waves in multilayer coating' were studied in the 1970s, both theoretically [3,4] and experimentally [5]. In the late 1990s, the excitation of PC SMs in a Kretschmann-like configuration was demonstrated [6].

PC SMs do not suffer from metal damping and therefore have a longer propagation length than SPs, which makes it possible to obtain a more sensitive biosensor. An additional advantage of the PC SM biosensor was demonstrated already in its first experimental realization [7]: it is the ability to detect both surface events and changes in volume refractive index independently. This feature also exists in a commercial version of this biosensor [8] and permits the segregation of the volume and the surface contributions from an analyte in detected signals [9–11].

On the other hand, the SPR technique has its imaging modification (SPRi), which was first demonstrated in the late 1980s by two groups: Yeatman and Ash [12] and Rothenhäusler and Knoll [13,14]. Although SPRi has attracted much attention recently [15], to the best of our knowledge, no imaging modification of optical biosensors based on PC SM has been proposed. The reason is straightforward: in a standard SPRi, the biochip surface is illuminated by a parallel light beam, the angle of incidence of which is tuned on the slope of the resonance dip in the SPR reflectivity curve. A two-dimensional (2D) black and white camera then detects the reflected intensity from each point on the investigated surface. Thus, the width of the angular SPR curve determines the dynamic range of the SPRi. However, PC SMs have a longer propagation length and a much smaller resonance angle curve width. Therefore, the dynamic range of the PC SM sensor in a similar scheme would be negligible and impractical.

In this article, we present a novel scheme and the practical implementation of a PC SM imaging (PC SMi) biosensor, with better

* Corresponding author.
E-mail address: konopsky@isan.troitsk.ru (V.N. Konopsky).

https://doi.org/10.1016/j.snb.2018.08.101
Received 9 April 2018; Received in revised form 20 August 2018; Accepted 21 August 2018
Available online 23 August 2018

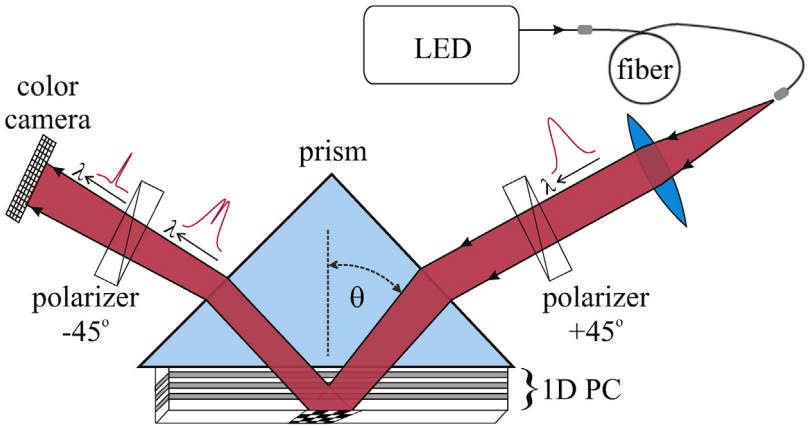

Fig. 1. Schematic of the biosensor. Typical spectra of the light as it passes from the LED to the color camera are shown.

dynamic range and thickness resolution than SPRi.

2. Materials and methods

2.1. PC SM imaging biosensor

A new 2D imaging biosensor with spectral registration of PC SM resonance shift is presented in this paper. Fig. 1 shows a schematic of the biosensor and typical spectra of an optical beam as it passes through the optical elements of the biosensor. A parallel light beam, with polarization $+45^{\circ}$ to the plane of incidence, illuminates a one-dimensional (1D) PC chip through a prism (Kretsch-mann-like configuration). After reflection, the light beam passes through the second polarizer, which is -45° to the plane of incidence, and is then recorded by a color camera (D1312C, Photonfocus, Lachen, Switzerland). Thus, the light beam passes through crossed polarizers and, if the PC SM does not undergo excitation, there is no signal at the color camera. However, we designed the 1D PC chip so that it supports a *p*-polarized PC SM at $\lambda = 500$ nm with an effective refractive index (RI) $\rho = 1.3825$, which corresponds to an in-prism excitation angle $\theta = 65.18^{\circ}$. A fiber-coupled LED (M505F1, Thorlabs, Newton, NJ, USA), with a peak wavelength near $\lambda = 500$ nm and a bandwidth (FWHM) of 35 nm, is used for excitation of the PC SM. This excitation causes a phase shift of the surface wave that re-radiates back to the prism. Therefore, rotation of the resulting polarization of the reflected beam occurs, and, as the result, the light at the excitation wavelength passes through the crossed polarizers.

The mean wavelength of the light that has passed through is determined by balancing of the intensities of the blue and green pixels at each point in the color camera. The structure of the 1D PC was designed so that the excitation wavelength of the PC SM is located between the maxima of the blue and green pixels. These spectral positions are illustrated schematically in Fig. 2. The figure shows that an increase (decrease) in the adsorption layer thickness d_a will cause a shift in the PC SM peak (Fig. 2, bottom) to longer (shorter) wavelengths, therefore increasing (decreasing) the green component and simultaneously decreasing (increasing) the blue component in the color pixel response.

Experimental spectra of the PC SM dip and peak are shown in Fig. 3. To register these spectra, the color camera in Fig. 1 was temporarily replaced by the fiber input of a fiber-coupled spectrometer (F30-EXR, Filmetrics, San Diego, CA, USA). The spectrum of the PC SM peak was recorded at the crossed polarizers, while the spectrum of the PC SM dip was recorded after removing the second polarizer and rotating the first polarizer for *p*-polarization transmission (0° to the plane of incidence). To record the spectra for different RIs of external media, water was replaced by 2% and 4% solutions of ethanol (EtOH). The increase in the RI of the external media led to a spectral shift of the PC SM dip and peak to longer wavelengths, as expected.

2.2. Photonic crystal structure

The 1D PC structure used in our experiments is: *substrate* /$H(LH)^5L'$/ *water*, where H is a TiO_2 layer (thickness $d_2 = 63.1$ nm), L is a SiO_2 layer (thickness $d_1 = 240.2$ nm), and L' is a final SiO_2 layer (thickness $d_3 = 341.0$ nm). The TiO_2/SiO_2 12-layer structure, with TiO_2 as the first layer and SiO_2 as the last layer, is coated by a SYRUSpro 710 optical vacuum coater (Buhler Leybold Optics, Alzenau, Germany) via electron-beam evaporation and plasma ion-assisted deposition. The prism and the glass plate substrate are BK-7 glass. At $\lambda = 500$ nm, the RIs of the substrate, SiO_2, TiO_2, and water are $n_0 = 1.521$, $n_1 = n_3 = 1.475$, $n_2 = 2.433$ and $n_e = 1.338$, respectively.

2.3. Reagents

The reagents used in the experiment were water, sodium chloride (NaCl), ethanol (EtOH), poly (allylamine hydrochloride) (PAH, 58 kDa), poly (styrene sulfonic acid), sodium salt (PSS, 77 kDa), poly (allylamine) solution (PAA, 65 kDa, 0.1 mg/mL), glutaraldehyde solution (GA, 100 Da, 0.1%), IgG from human serum, Anti-Human IgG antibody produced in rabbit (polyclonal, 2.5 mg/mL), Anti-Bovine Albumin antibody produced in rabbit (polyclonal, 3.0 mg/mL). Three last reagent were used in dilution of 1:100. All reagents were purchased from Sigma–Aldrich (St. Louis, MO, USA).

2.4. Sample preparation

A PC chip was washed twice in an ultrasonic bath of pure EtOH solution (each bath was 10 min) and then treated with a home-made UV/ozone cleaner (15 min) immediately before use. The treatment makes the chip hydrophilic, with expected *OH* bonds on the negatively charged SiO_2 surface. For multiplexed antigen/antibody experiments, hydrophilic PC chips were preliminary immersed into water solutions of PAA and GA for five minutes, followed by water rinsing (before spots deposition) [10].

2.5. Data handling

Data acquired by the color camera was processed and presented using custom software. The shift of the PC SM resonance wavelength was determined from the next normalized differential value:

$$z(x, y) = \frac{B(x, y) - G(x, y)}{B(x, y) + G(x, y)}, \quad (1)$$

where $B(x, y)$ and $G(x, y)$ are the intensities of the blue and green components in each color pixel (x, y) of the camera.

To convert $z(x, y)$ into $\lambda(x, y)$, the responsivities of the color camera must be known. They are not the ideal Gaussian curve, as shown

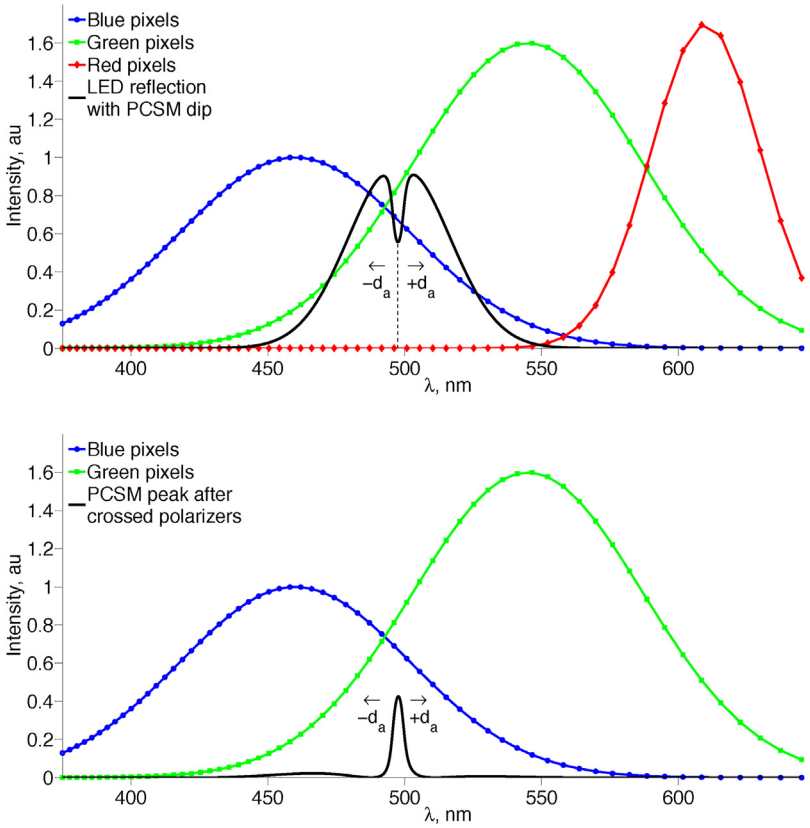

Fig. 2. Theoretical calculation of the PC SM dip (top) and peak (bottom) in the spectrum of the reflected LED light. Spectral responsivities of red, green, and blue pixels for a typical color camera are schematically presented using corresponding colors. (For interpretation of the references to color in this figure legend, the reader is referred to the web version of this article.)

schematically in Fig. 2. The real responsivities of the green and blue pixels of our camera (D1312C), provided by the manufacturer, are presented in Fig. 4 (top).

The normalized difference z, calculated using these real responsivities, is presented in Fig. 4 (middle), which shows that the real $z(\lambda)$ is not perfectly linear, even near $z \sim 0$. To correct this problem, the inverse value $\lambda(z)$ undergoes a polynomial fit:

$$\lambda(z) = \sum_{n=0}^{n=8} p_n \cdot z^n, \tag{2}$$

the result of which is shown in Fig. 4 (bottom) by the solid line for the next coefficients: $p_{[0\rightarrow 8]} = [494; -40.5; -48.8; -165.2; 101.9; 716; 94.5; -951; -437.3]$. Now, after obtaining the experimental data from the color camera, we used Eq. (1) to determine z and then Eq. (2) to determine λ for each camera pixel to obtain the spatial distribution $\lambda(x, y)$ across the camera that reflects the spatial distribution of the PC SM resonance shifts across the sample.

3. Results

3.1. Detection of changes in volume RI

For an initial test of the biosensor, 4% and 12% EtOH solutions were injected into a flow cell, alternating with pure water injections. Fig. 5 presents the signals from the wavelength shifts ($\Delta\lambda$). Note that our data-handling procedure using Eqs. (1) and (2) yielded (for the 4% solution) $\Delta\lambda = 0.6$ nm, which coincides exactly with the wavelength shifts measured directly by the spectrometer (see Fig. 3) for a solution with the same concentration.

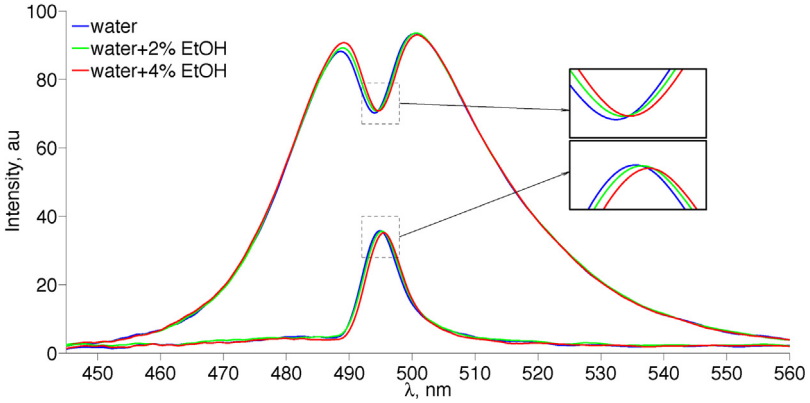

Fig. 3. Experimental spectra of the PC SM dips and peaks for three different solutions. Insets show enlarged views of the shifts due to changes in the RI with change in solution.

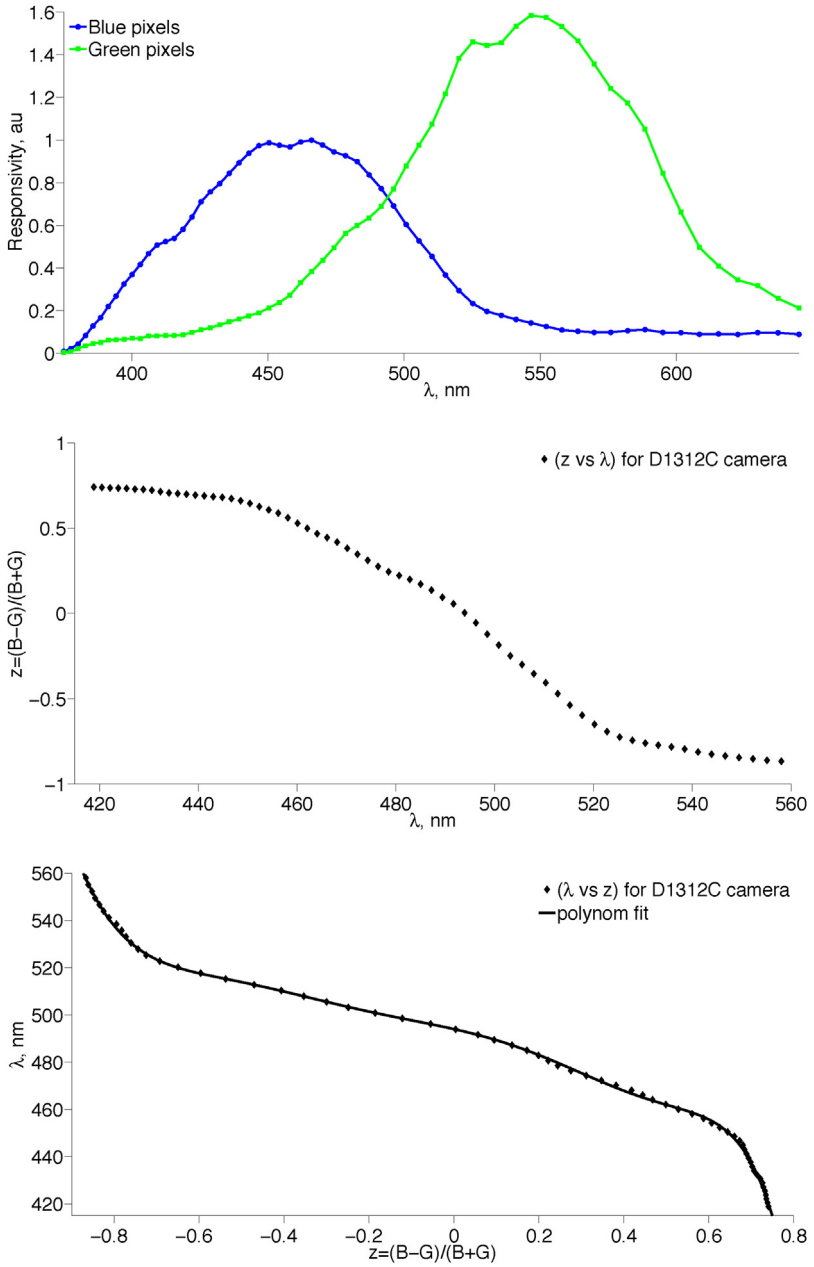

Fig. 4. Responsivities of the blue and green pixels of the color camera D1312C (top), their normalized difference (middle), and the inverse function λ(z) with their polynomial fit (bottom). (For interpretation of the references to color in this figure legend, the reader is referred to the web version of this article.)

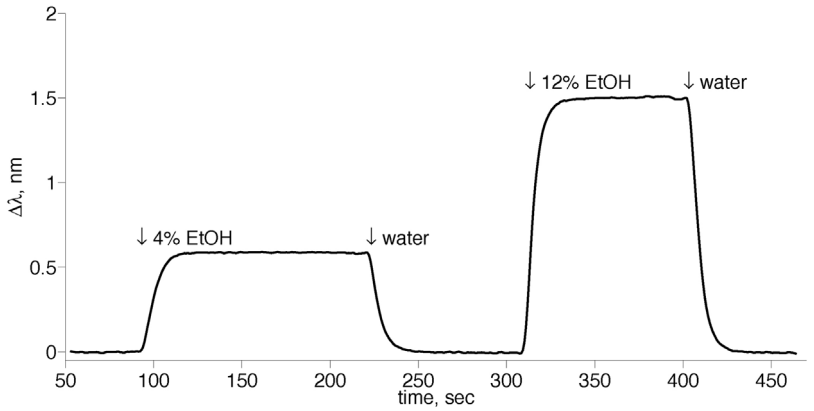

Fig. 5. PC SM resonance shifts resulting from changes in volume RI.

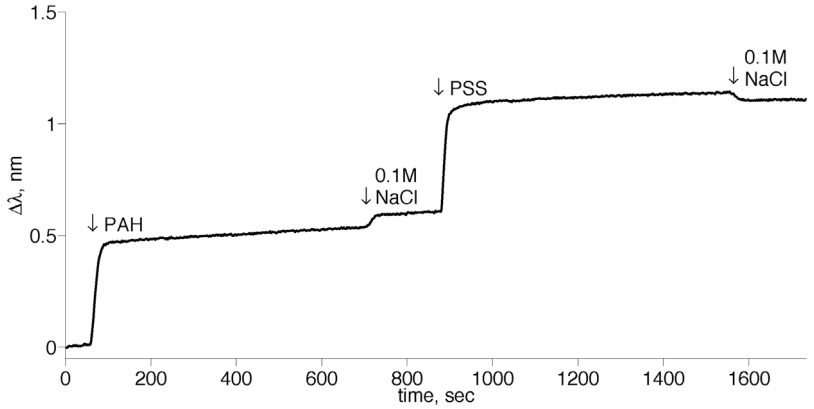

Fig. 6. PC SM resonance shifts due to deposition of polyelectrolytes on the surface of the biosensor.

3.2. Deposition of PAH and PSS polyelectrolytes

A polyelectrolyte sandwich was prepared using the positive polyelectrolyte PAH and the negative polyelectrolyte PSS, both at 1 mM concentration (calculated with respect to the monomer) in an aqueous solution of 0.1 M NaCl. The PC SM chip was mounted onto the flow cell of the PC SM instrument immediately after UV/ozone treatment that resulted with the expected negatively charged SiO_2 surface.

The chip was alternately exposed to the PAH and PSS solutions for 10 min, starting with the positive polyelectrolyte PAH. After each adsorption step, the substrate was rinsed with an aqueous solution of 0.1 M NaCl for 100 s before exposure to next electrolyte solution. The results are presented in Fig. 6.

3.3. Test images registrations

The two images in Fig. 7 demonstrate the 2D imaging capability of the biosensor. We lightly pressed a rubber stamp dampened with PAH onto the freshly cleaned PC chip. The positively charged PAH bonded with the negatively charged SiO_2 surface to produce a nanometer-thick pattern that was easily detected by the imaging biosensor. The characters "EVA 3.0″ engraved on the stamp (see Fig. 7, bottom left) were revealed immediately after placing the PC chip into the water-filled liquid cell and remained visible after the subsequent deposition of five PSS/PAH layers using the protocol described in Section 3.2. The top-left image in Fig. 7 shows that the deposition of multiple layers increased the overall thickness but the characters remained thicker and visible. The spectral positions of the PC SM resonance in the spatial locations, indicated by arrows, were $\lambda_1 = 494.86$ nm and $\lambda_2 = 494.37$ nm, with the difference between them $\Delta\lambda = 0.49$ nm.

The second stamp used in our experiment contained a square grid with a 300 μm pitch (widths of the hole and the bar both 150 μm). Fig. 7 (right) is an enlarged view of part of the PC chip image, showing that the spatial resolution of the biosensor is about 100 μm. In addition, the decimal point between the "3" and the "0", the diameter of which was 130 μm (image on the left side of Fig. 7) is also visible. The propagation length of the surface mode in the chosen PC structure always restricts the minimal spatial resolution of the technique presented here. However, even if using spots with a 600-μm-pitch and a 300-μm diameter, about 1000 spots can be deposited on the PC chip with a working area of 18 × 18 mm^2. That number of spots is more than enough for most applications.

3.4. Multispots binding of Human/Anti-Human IgG.

To demonstrate multiplexing potential of the proposed approach, we recorded a test binding reaction where the antibody (Human IgG), immobilized on the PC surface, serves as biological recognition element. Forty-two spots were deposited on PC sensor surface: twenty-one Anti-BSA spots (as a control) and twenty-one spots of Human-IgG. Spots were applied to the surface by a needle bundle, where 3 × 7 needles were tied together and their tips were blunted by polishing. The 3 × 7 needle bundle was immersed in a napkin, impregnated with Anti-BSA or Human-IgG, respectively, and then slightly touched the surface of PC chip, preliminary coated by PAA and GA layers.

The result of deposition is shown in Fig. 8 (top left). One can see that spots have a 1-mm-pitch and a 400-μm diameter. Images are squeezed horizontally in a ratio of about 2:1, since they appear on the camera after reflection inside the prism at the angle $\theta = 65.18^{\circ}$. Thus, round spots are seen as elliptical. The degree of darkening in the upper images in Fig. 8 is related to the normalized differential value $z(x, y)$ (see Eq. (1)).

Both upper images were recorded in pure water: the left one before the Anti-Human IgG injection, while the right one after the injection and pure water flushing. The bottom diagram shows the kinetics of this process in one particular spot (labelled by white rectangles). In Appendix A one can find the complete video of transformations of the images during this process.

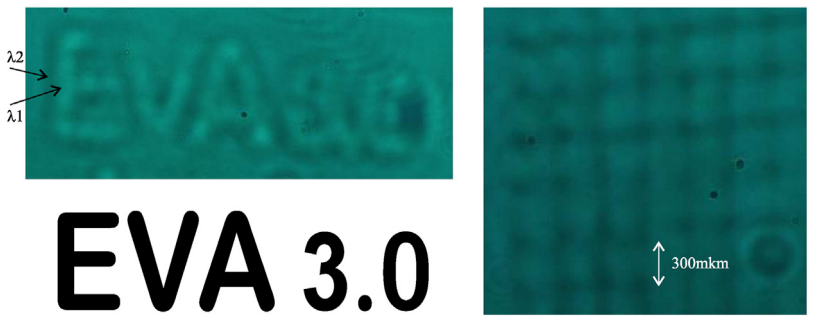

Fig. 7. 2D view of the surface of the PC chip onto which images with the thickness of one PAH layer were deposited by stamp printing: "EVA 3.0″ (left) and test square grid with 300-μm pitch (right).

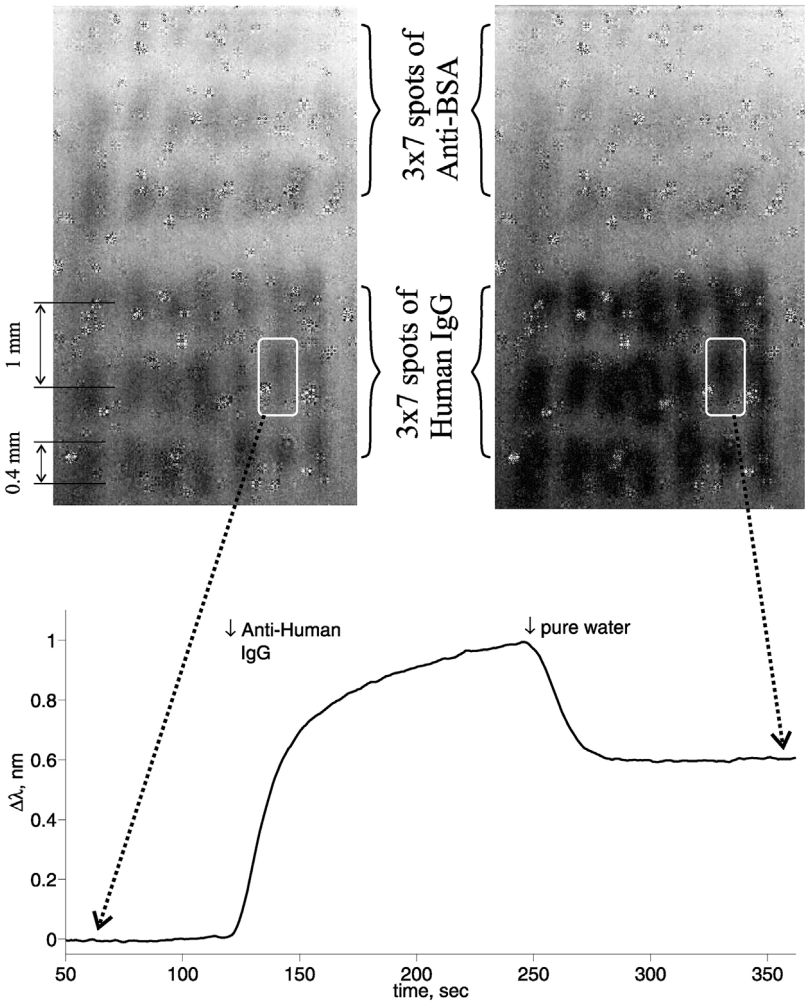

Fig. 8. Images of 21 spots of Anti-BSA and 21 spots of Human IgG before (top left) and after (top right) the water rinsing following by the injection of Anti-Human IgG. The kinetics of the process of (Human IgG)/(Anti-Human IgG) binding in a particular spot is also presented (buttom). Full video of the process may be found in Appendix A.

4. Discussion

4.1. Principles of 2D-imaging biosensor operation

A common problem in biosensor imaging is that one spatial dimension of the camera is usually used for signal registration, leaving only one dimension for the detection of spatial variations of the signal (1D imaging). For example, in wavelength-interrogation techniques, one dimension of the camera is used to detect the spectrum and the other dimension may be used to detect the spatial variations of the spectral signal (1D-imaging spectroscopy). In angular-interrogation techniques, again, one dimension is used to detect shifts of a resonance angle (sometimes with additional detection of the total internal reflection angle [16,17]) and the other dimension is used to detect spatial variations of the angular signals.

To obtain a 2D image, both dimensions of the camera matrix should be used to detect spatial variables. Therefore, a pixel value itself must be used as a signal value. Indeed, SPRi uses intensity interrogation to obtain 2D data on surface plasmon resonances. In our approach, the color components of each pixel are used to obtain a 2D image that reflects the spectral shifts of PC SM resonances across the surface under study.

It should be noted that exactly the same approach is impossible for SPR registration because of the large spectral resonance width of surface plasmons, which is due to the high optical losses that occur in metal films. Nevertheless, there were attempts to use the color camera for detection of spectral variations in the wide SPR reflection curve [18,19]. In these SPRi modifications the Hue (H) component of HSV color coding (obtaining from RGB colors by nonlinear conversion) was used as the signal value, since only the Hue component directly refers to the dominant color wavelength. There were no noticeable SPR peaks there, and the Hue component was basically changed in result of variations in reflected intensity in red and infra-red spectral regions. In our PC SMi biosensor the signal value is obtained from the spectral shift of the narrow resonance peak by Eqs. (1) and (2), which is more straightforward and gives a more linear response and much larger dynamic range. So, the often-mentioned advantage of PC SM, namely, low optical losses and narrow spectral resonance widths, is really important here and allows the creation of such an image-forming device.

Moreover, the narrowness of the spectral peak of PC SM reduces the requirement for the spectral stability of the LED in our setup. For example, if, due to some temperature changes, a drift of the central wavelength of the LED takes place, this will lead to a change of the intensity of the PC SM peak only. But the change of the PC SM peak intensity (due to the spectral drifts or intensity noises of LED) is irrelevant, since Eq. (1) is the normalized difference, and, therefore, the intensity changes of the light source will be suppressed after Eq. (1) execution.

Besides low loss, the PC SMs have such additional advantage as the possibility to design a 1D PC, whose surface would support the PC SM at

any preliminarily chosen wavelength. In this study, this possibility was used to tune the PC SM excitation wavelength to spectral region near 500 nm. This wavelength is located between the maximum responsivities for the blue (~460 nm) and green (~545 nm) pixels of the color camera. Therefore, the 500-nm wavelength is located on the descending and ascending slopes of the responsivity curves of the blue and green pixels, respectively. To obtain the PC SM at a predetermined wavelength ($\lambda = 500$ nm) with a predetermined effective RI ($\rho = 1.3825$), we used the design algorithm described by one of us earlier [20].

4.2. Conversion of resonance dip into resonance peak using two polarizers

Working with a resonance peak instead of a resonance dip makes it possible to increase the signal-to-noise ratio and reduce the need for the spectral stability of the LED (as mentioned above). Our preliminary experiments with the registration of resonance dip (i.e., without the crossed polarizers) show that indeed the signal-to-noise ratio is better for the resonance peak registration.

To understand how it is possible to convert a resonance dip into a resonance peak, note that the dip in a reflection curve (for both SPR and PC SM) is the result of destructive interference between two beams. One beam is reflected off the internal interface between a glass prism and a surface-wave-supporting film (metal film for SPR and multilayer film for PC SM), and the second beam, which is from the surface wave on the external interface of the film, is reradiated back to the prism with phase shift π. These two beams undergo destructive interference and the resonance dip appears. If the incoming beam is polarized at +45° to the plane of incidence, then its *p*-polarized part has components that are phase-shifted after reflection (if surface wave excitation occurs), while its *s*-polarized part is reflected without any prominent phase shift. Therefore, the resulting polarization will have a component with its polarization rotated from +45° to −45° after reflection. It will be the component that passed through surface wave excitation resulting in the phase shift π. The second polarizer transmits only this component and blocks all light that does not take part in the excitation of the surface wave. Thus, only the light reradiated from the surface mode survives after the second polarizer.

It worth to note that to obtain similar (but much wider) SPR peak at a plasmon resonance wavelength in the red or infrared region, an additional phase plate should be inserted between crossed polarizers, since, after reflection from the metal film, the *s*-polarization also has a noticeable constant phase shift [21].

4.3. Sensor sensitivities and baseline noise

The biosensor reveals volume and surface changes as a shift in resonance, in nanometers (of wavelength). To convert the shift to refractive index units (RIU) or to changes in the adsorbate layer thickness in nanometers (of thickness), additional calculations of correspondent sensitivities are needed. In addition, after multiplying the sensitivities by baseline noise, which is $\delta\lambda = 10^{-3}$ nm in the present device (for 1-s accumulation time and for the minimal spot size ~100 × 100 μm^2), the baseline noise of the device in units of volume RI or adlayer thickness may be obtained (during the integration over this minimal spot size). It should be noted that if spatial integration takes place over a large spot size (> 1 cm^2), the baseline noise is an order of magnitude smaller ($\delta\lambda = 10^{-4}$ nm), and the baseline noises of n_e and d_a, measured over large spots, is also accordingly smaller.

4.3.1. In units of volume RI

Theoretical calculations of the spectral shift of the PC SM in our device yield a value of sensitivity to changes in volume RI $\Delta\lambda/\Delta n_e = 393$ nm/RIU. Therefore, the baseline noise in RIU is $\delta n_e = 2.5 \times 10^{-6}$ during the integration over the minimal spot size and is $\delta n_e = 2.5 \times 10^{-7}$ during the integration over the larger spot sizes.

4.3.2. In units of adsorbate thickness

To calculate the spectral shift of the PC SM that is due to changes in adlayer thickness, it is assumed that the RI of the adlayer is $n_a = 1.43$, which yields a sensitivity to changes in adlayer thickness of $\Delta\lambda/\Delta d_a = 0.284$ nm/nm. Therefore, the baseline noise in thickness units is $\delta d_a = 3.5 \times 10^{-3}$ nm = 3.5 pm, which corresponds to 3.5 pg/mm^2 in surface mass density. For the highest spatial resolution it gives 35 fg, which is deposited in the spot 100 × 100 μm^2.

4.4. Dynamic range

The dynamic range (DR) of the current biosensor is limited by the LED bandwidth, which is 35 nm (FWHM). Thus, the operating range of the device is 480–515 nm. To obtain the DR, the corresponding RI or the change in thickness that shifts the PC SM from 480 to 515 nm is used. For our device, the DR is $^{515}_{480}\Delta n_e \simeq 0.05$RIU or $^{515}_{480}\Delta d_a \simeq 150$ nm. If a light source with a wider spectrum will be used, the DR can be two to three times larger (450–550 nm) and will be limited only by the spectral range between the maxima of the blue and green pixels (see Fig. 4).

4.5. Comparison with commersial SPRi devices

At the end of this section, we make a brief comparison with three SPRi devices from the GWC Technologies and the HORIBA Scientific.

The GWC Technologies releases SPRi instrument with the limit of detection 8 pg/mm^2 and spatial resolution 25 μm (with recommendation to use probe spots at least 100 μm in diameter) [22,23]. The DR of GWC Technologies biosensor is $\Delta n_e \simeq 0.04$RIU and corresponds to a 10% change in reflectivity on the slope of the SPR curve [23].

The HORIBA Scientific produces two SPRi instruments: OpenPlex and XelPleX [24] with detection limits: 10 pg/mm^2 and 5 pg/mm^2, respectively. One can see that the SPRi devices have better spatial resolution – as expected, because the surface plasmons have a shorter propagation length. On the other hand, even our first prototype version of PC SMi has better detection limit and dynamic range.

5. Conclusions

In this paper, we presented a new biosensor technique capable of 2D imaging of a biosensor surface with a spatial resolution of about 100 μm, and made experimental tests of the technique. An analysis of the principles of operation of the device and the initial experiments using the device showed that the proposed imaging method can surpass its plasmonic analog (SPRi) with respect to both signal-to-noise ratio and dynamic range.

Appendix A. Supplementary data

Video file that illustrates process of Anti-Human IgG binding to Human IgG spots is presented in Supplementary data.

Acknowledgement

This research did not receive any specific grants from any funding agencies. The authors are grateful to Dmitry Basmanov for assistance in the preparation of experiments of antigen/antibody binding.

Appendix A. Supplementary data

Supplementary data associated with this article can be found, in the online version, at https://doi.org/10.1016/j.snb.2018.08.101.

References

[1] X. Fan, I.M. White, S.I. Shopoua, H. Zhu, J.D. Suter, Y. Sun, Sensitive optical biosensors for unlabeled targets: a review, Anal. Chim. Acta 620 (1–2) (2008) 8–26.

[2] J. Homola, Surface plasmon resonance sensors for detection of chemical and biological species, Chem. Rev. 108 (2) (2008) 462–493.
[3] J.A. Arnaud, A.A.M. Saleh, Guidance of surface waves by multilayer coatings, Appl. Opt. 13 (1974) 2343–2345.
[4] P. Yeh, A. Yariv, C.-S. Hong, Electromagnetic propagation in periodic stratified media. I. General theory, J. Opt. Soc. Am. 67 (4) (1977) 423–438.
[5] P. Yeh, A. Yariv, A.Y. Cho, Optical surface waves in periodic layered media, Appl. Phys. Lett. 32 (2) (1978) 104–105.
[6] W.M. Robertson, M.S. May, Surface electromagnetic waves on one-dimensional photonic band gap arrays, Appl. Phys. Lett. 74 (13) (1999) 1800–1802.
[7] V.N. Konopsky, E.V. Alieva, Photonic crystal surface waves for optical biosensors, Anal. Chem. 79 (12) (2007) 4729–4735.
[8] http://www.pcbiosensors.com (2011).
[9] V.N. Konopsky, T. Karakouz, E.V. Alieva, C. Vicario, S.K. Sekatskii, G. Dietler, Photonic crystal biosensor based on optical surface waves, Sensors 13 (2) (2013) 2566–2578.
[10] O. Tatarinova, V. Tsvetkov, D. Basmanov, N. Barinov, I. Smirnov, E. Timofeev, D. Kaluzhny, A. Chuvilin, D. Klinov, A. Varizhuk, G. Pozmogova, Comparison of the “chemical” and “structural” approaches to the optimization of the thrombin-binding aptamer, PLOS ONE 9 (2) (2014) e89383.
[11] M. Prokofjeva, V. Tsvetkov, D. Basmanov, A. Varizhuk, M. Lagarkova, I. Smirnov, K. Prusakov, D. Klinov, V. Prassolov, G. Pozmogova, S. Mikhailov, Anti-hiv activities of intramolecular g4 and non-g4 oligonucleotides, Nucl. Acid Ther. 27 (1) (2017) 56–66.
[12] E. Yeatman, E. Ash, Surface plasmon microscopy, Electron. Lett. 23 (20) (1987) 1091–1092.
[13] B. Rothenhäusler, C. Duschl, W. Knoll, Plasmon surface polariton fields for the characterization of thin films, Thin Solid Films 159 (1–2) (1988) 323–330.
[14] B. Rothenhäusler, W. Knoll, Surface plasmon microscopy, Nature 332 (6165) (1988) 615–617.
[15] P. Singh, SPR biosensors: historical perspectives and current challenges, Sens. Actuators B: Chem. 229 (2016) 110–130.
[16] V.N. Konopsky, E.V. Alieva, A biosensor based on photonic crystal surface waves with an independent registration of the liquid refractive index, Biosens. Bioelectron. 25 (5) (2010) 1212–1216.
[17] V.N. Konopsky, E.V. Alieva, Critical-angle refractometer enhanced by periodic multilayer coating, Sens. Actuator B-Chem. 150 (2010) 794–797.
[18] H. Ho, C. Wong, K. Chan, S. Wu, C. Lin, Application of two-dimensional spectral surface plasmon resonance to imaging of pressure distribution in elastohydrodynamic lubricant films, Appl. Optics 45 (23) (2006) 5819–5826.
[19] C.L. Wong, G.C.K. Chen, B.K. Ng, S. Agarwal, Z. Lin, P. Chen, H.P. Ho, Multiplex spectral surface plasmon resonance imaging (spri) sensor based on the polarization control scheme, Opt. Express 19 (20) (2011) 18965–18978.
[20] V.N. Konopsky, Plasmon-polariton waves in nanofilms on one-dimensional photonic crystal surfaces, New J. Phys. 12 (2010) 093006.
[21] J. Homola, S.S. Yee, Novel polarization control scheme for spectral surface plasmon resonance sensors, Sens. Actuators B: Chem. 51 (1) (1998) 331–339.
[22] B.P. Nelson, T.E. Grimsrud, M.R. Liles, R.M. Goodman, R.M. Corn, Surface plasmon resonance imaging measurements of DNA and RNA hybridization adsorption onto DNA microarrays, Anal. Chem. 73 (1) (2001) 1–7.
[23] http://www.gwctechnologies.com/pdfs/123-sensitivity.pdf.
[24] http://www.horiba.com.

Valery N. Konopsky received the Ph.D. and M.S. degrees from the Moscow Institute of Physics and Technology in 1996 and 1993, respectively. During 1990–1993 he worked at Lebedev Physical Institute in Moscow and then, during 1993–1996, he worked at the Institute of Spectroscopy in Troitsk. Since 1996 he is a staff member of the Institute of Spectroscopy and currently he is a Senior Scientific Researcher, headed a group that is active in optical investigation of surfaces and surface nanostructures. His present research interests include surface optical waves, optical chemical sensors and biosensors.

Elena V. Alieva received the M.S. degrees from the Moscow Institute of Physics and Technology in 1976 and received her PhD in Physics and Mathematics from the Institute of Spectroscopy, Russian Academy of Sciences in 1980. Since 1988 she is a Senior Scientific Researcher at the Institute of Spectroscopy. Her current research interests include surface optics, surface electromagnetic waves and spectroscopy of surfaces and thin films.